



21st century change in precipitation on the Greenland Ice Sheet using high resolution regional climate models

Fredrik Boberg¹, Nicolaj Hansen¹, Ruth Mottram¹, Xavier Fettweis², Michiel R. van den Broeke³

¹National Centre for Climate Research, Danish Meteorological Institute (DMI), Copenhagen, Denmark ²Laboratory of Climatology, SPHERES research unit, Geography Department, University of Liège, Liège, Belgium ³Institute for Marine and Atmospheric Research (IMAU), Utrecht University, Utrecht, The Netherlands

Correspondence to: Fredrik Boberg (<u>fbo@dmi.dk</u>)

Abstract. An ensemble of regional climate model simulations downscaling global climate models within Coupled Model Intercomparison Project Phase 6 (CMIP6) is used to estimate future precipitation changes for the Greenland ice sheet under a range of climate change pathways. The regional climate models are HIRHAM5, MAR3.12 and RACMO2.3p2 contributing a total of eleven simulations for the SSP5-8.5 scenario, five simulations for the SSP2-4.5 scenario and four simulations for the SSP1-2.6 scenario. The Greenland ice sheet is divided into six drainage basins to evaluate the change in total (snow plus rain) precipitation in regions with different precipitation characteristics. Compared with the reference period 1971-2000, the ensemble median change in precipitation for the full Greenland ice sheet for the SSP5-8.5 scenario is estimated to be about +60 Gt (+8%) per year during the 2031-2060 period and +170 Gt (+24%) per year during the 2071-2100 period. We see similar ensemble median change for the 2031-2060 period for the SSP1-2.6 and SSP2-4.5 scenarios while the 2071-2100 change is +40 and +80 Gt (+6 and +11%) per year for SSP1-2.6 and SSP2-4.5, respectively. In contrast to this, recent studies show that runoff is projected to increase by a much larger amount (around 2,000 Gt per year for the end of this century). Using linear regression on the annual mean change in near-surface (2 m) air temperature and precipitation over the ice sheet, we estimate an increase of about 35 Gt per year in precipitation (equal to about 5%) for every degree of warming during the 21st century. We also study the change in phase of the total precipitation, showing a relative increase in rainfall, particularly along the outer edge and the southern part of the ice sheet. The regional climate model output is compared with an ensemble of global climate models within CMIP6 showing similar patterns in precipitation change but with overall larger changes in the CMIP6 ensemble median compared with the regional climate model ensemble median.

1 Introduction

Solid precipitation (snowfall) is the largest positive contributor to the (surface) mass balance of the Greenland ice sheet (GrIS).

Runoff from the Greenland ice sheet is the largest negative surface mass balance component and currently a main contributor to sea level rise (Box et al., 2022). Early work (Huybrechts et al., 1991) suggested that the GrIS would not contribute significantly to future sea level rise because of the projected increase in snowfall, compensating for increased runoff. However,





the observed increase in surface melt/runoff and ice dynamic changes leading to increased solid ice discharge since the late 1990s shows conclusively that, in spite of an increase in observed precipitation (Box et al., 2022), the GrIS is net losing mass as increases in melt and runoff rates outpace increases in snowfall. The accumulation of snow is not only important for the ice sheet mass balance (the sum of surface mass balance and solid ice discharge) but also has process implications for ablation via surface albedo feedbacks and firn pore space and energy budgets that determine the retention and refreezing of melt water in the firn pack (Firn Symposium team, 2024; Glaude et al., 2024). If warming-enhanced precipitation occurs under future climate change scenarios, it is likewise important to determine the phase. Liquid precipitation percolates into near-surface snow/firn layers and thereby decreases the pore space in the firn. The higher temperature of rain compared to melt water also transports energy deeper into the firn, warming it and reducing refreezing potential. Where fresh snow generally increases surface albedo, rain usually has a darkening effect on surface snow, particularly in near infrared wavelengths, and can therefore also enhance melt-albedo feedbacks. On bare glacier ice in the absence of snow though, rain can also increase albedo, by washing away surface debris and biological crusts.

Huai et al. (2025) used CMIP5 and CMIP6 ensembles and found a model mean increase in precipitation for the entire GrIS during the 21st century with changes in excess of 200 mm yr⁻¹ along the outer edges for the SSP5-8.5 scenario. However, some individual models showed a decrease in the southeast. Bochow et al. (2024) used CMIP6 ensembles for four different emission scenarios and found an increase in precipitation in correlation with the increase in surface temperature for the 21st century. The aim of this study is to study changes (amount and phase) in the GrIS precipitation for the 21st century using an ensemble of high resolution regional climate model simulations and compare these results with the forcing CMIP6 models.

2 Data

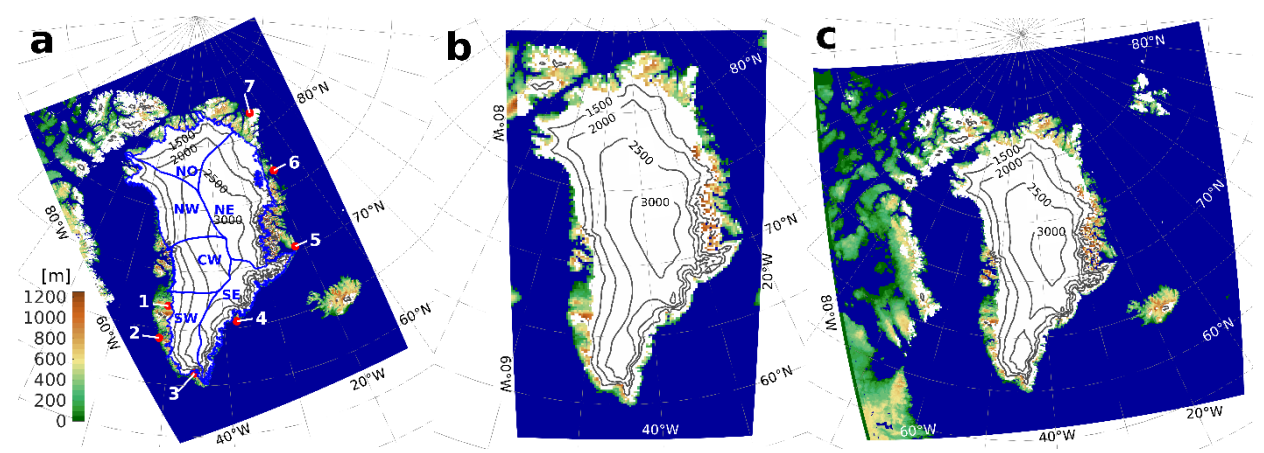


Figure 1: Model domain and orography for the HIRHAM (a), MAR (b) and RACMO (c) RCM simulations. Sea points are given in blue, glacier free land points in green/brown and glacier points in white with added surface elevation contour lines in black. The

© Author(s) 2025. CC BY 4.0 License.





location of seven observational stations (red dots) and six drainage basins (blue contour lines; Rignot and Mouginot, 2012) are shown in panel a. The stations in order 1–7 are Kangerlussuaq, Nuuk, Narsarsuaq, Tasiilaq, Ittoqqortoormiit, Danmarkshavn and Station Nord.

2.1 Models

60

A total of eleven global climate model (GCM) – regional climate model (RCM) combinations are used in this study. The RCMs used are: HIRHAM5 (from now on: HIRHAM; one SSP1-2.6 and two SSP5-8.5 simulations), MAR3.12 (from now on: MAR; two SSP1-2.6, four SSP2-4.5 and eight SSP5-8.5 simulations) and RACMO2 (from now on: RACMO; one for each of the three SSP scenarios) (see Table 1). The reference period for this study is 1971–2000, taken from the historical run of the RCM simulations. Two future periods (2031–2060 and 2071–2100) are extracted from the three SSP scenarios. We use the period 1991–2022, using data for both the historical period (from 1991 to 2014) and the SSP5-8.5 period (from 2015 to 2022), for model evaluation against observations and reanalysis data.

The two HIRHAM (combining the dynamics of the HIRLAM model (Undén et al., 2002) and the physical parameterization schemes of the ECHAM model (Roeckner et al., 2003)) simulations are performed on a rotated latitude-longitude grid with a horizontal resolution of 0.05° (about 5.5 km) (Figure 1a; cf. Boberg et al. (2022) for a more detailed model setup description). The first HIRHAM simulation is forced with the CMIP6 GCM EC-Earth3 for the period 1970–2100 (where the first year is used for spin-up) using the SSP1-2.6 and SSP5-8.5 scenarios whereas the second HIRHAM simulation is forced by CMIP6 GCM CESM2-L for the SSP5-8.5 scenario and the same model set-up and period as for the HIRHAM/EC-Earth3 simulation.

The MAR (Modéle Atmosphérique Régional) simulations (Figure 1b; Hofer et al., 2020) are performed with a horizontal resolution of 15 km. The CMIP6 GCMs that are downscaled with MAR are CESM2, CESM2-L, CNRM-CM6, CNRM-ESM2, IPSL-CM6A-LR, MPI-ESM1.2-HR, NorESM2 and UKESM1.0-LL. There are in total two SSP1-2.6 simulations, four SSP2-4.5 simulations and eight SSP5-8.5 simulations. The MAR data are regridded onto the HIRHAM grid to enable a model ensemble comparison (see Glaude et al., 2024). After regridding, we apply a common HIRHAM ice mask to all data since the GrIS extent for the three RCMs are comparable in size (within ±0.6%).

The RACMO simulations (Noël et al., 2020) are forced by CESM2-L and run at a horizontal resolution of 11 km (see Figure 1c) with one simulation per SSP scenario. The RACMO data are also regridded onto the HIRHAM grid. For a more detailed model description of RACMO, see Noël et al. (2018).

The RCM ensemble is compared with 34 CMIP6 GCM simulations (see Table 2) for the historical and the SSP5-8.5 scenario, selecting only one realization per GCM. The GCM output are regridded onto the EC-Earth3 grid with a horizontal resolution of about 80 km (Döscher et al., 2022).





Model	Res. [km]	P 1971– 2000 [Gt]	P 2031– 2060 [Gt]	P 2071– 2100 [Gt]	ΔP 2031- 2060		ΔP 2071- 2100		RMSE 1991–2022	Bias 1991–2022
					[Gt]	[%]	[Gt]	[%]	[mm]	[mm]
CARRA	2.5	842	N/A	N/A	N/A	N/A	N/A	N/A	188	-88
HIRHAM/EC-Earth3	5.5	751	835 N/A 863	883 N/A 1014	84 N/A 112	11 N/A 15	132 N/A 263	18 N/A 35	125	-10
HIRHAM/CESM2-L	5.5	762	N/A N/A 765	N/A N/A 931	N/A N/A 3	N/A N/A 0	N/A N/A 170	N/A N/A 22	199	106
RACMO/CESM2-L	11	700	744 717 715	696 720 849	40 17 15	6 2 2	-4 20 148	-1 3 21	352	109
MAR/CESM2	15	671	774 742 752	716 752 845	103 71 81	15 11 12	45 81 174	7 12 26	456	-290
MAR/CESM2-L	15	697	N/A N/A 708	N/A N/A 835	N/A N/A 11	N/A N/A 2	N/A N/A 139	N/A N/A 20	475	-312
MAR/CNRM-CM6	15	703	N/A N/A 754	N/A N/A 896	N/A N/A 51	N/A N/A 7	N/A N/A 193	N/A N/A 27	529	-386
MAR/CNRM-ESM2	15	696	N/A N/A 720	N/A N/A 815	N/A N/A 24	N/A N/A	N/A N/A 119	N/A N/A 17	514	-373
MAR/IPSL-CM6	15	703	N/A N/A 799	N/A N/A 957	N/A N/A 97	N/A N/A 14	N/A N/A 255	N/A N/A 36	598	-439
MAR/MPI-ESM1,2	15	690	726 721 746	720 766 845	36 31 56	5 4 8	30 76 155	4 11 22	548	-383
MAR/NorESM2	15	714	N/A 778 805	N/A 795 852	N/A 64 91	N/A 9 13	N/A 81 138	N/A 11 19	422	-233
MAR/UKESM1.0	15	684	N/A 824 855	N/A 954 1043	N/A 140 171	N/A 20 25	N/A 270 359	N/A 39 52	494	-322
Ensemble median	N/A	700	759 742 754	718 766 852	62 64 56	9 9 8	38 81 170	6 11 24	473	-307

Table 1: List of CARRA and the RCM simulations used in this study and the annual mean total precipitation for the GrIS for the reference period, the mid-century period and the end of century period. Also given are the absolute and relative changes for the two scenario periods. Numbers in blue/green/red are for the SSP1-2.6/SSP2-4.5/SSP5-8.5 scenario. Note that the CARRA value is for the period 1991–2022. Also given are the RMSEs and mean biases for 1991–2022 (using historical data and SSP5-8.5 data) relative to observations for the seven weather stations (cf. Figure 3).

GCM	P [Gt]	ΔP [Gt]	GCM	P [Gt]	ΔP [Gt]	GCM	P [Gt]	ΔP [Gt]
ACCESS-CM2	575	243	CNRM-CM6-1-HR	799	337	KACE-1-0-G	583	176
ACCESS-ESM1-5	590	287	CNRM-ESM2-1	882	156	MIROC6	771	180
AWI-CM-1-1-MR	655	242	E3SM-1-1	699	832	MIROC-ES2L	830	230
AWI-ESM-1-REcoM	663	253	EC-Earth3	702	320	MPI-ESM1-2-	634	159
						HR		

© Author(s) 2025. CC BY 4.0 License.



100

105

110

115

120



BCC-CSM2-MR	718	237	EC-Earth3-Veg	720	322	MPI-ESM1-2-LR	668	206
CAMS-CSM1-0	574	75	FGOALS-f3-L	690	260	MRI-ESM2-0	887	218
CanESM5-1	606	540	FGOALS-g3	740	72	NESM3	581	340
CESM2	805	128	FIO-ESM-2-0	687	247	NorESM2-MM	641	127
CESM2-WACCM	780	165	GFDL-ESM4	665	119	TaiESM1	717	183
CMCC-CM2-SR5	723	344	INM-CM4-8	655	172	UKESM1-0-LL	548	333
CMCC-ESM2	709	281	INM-CM5-0	677	204	Ensemble	CO 4	222
CNRM-CM6-1	848	196	IPSL-CM6A-LR	853	393	median	694	233

Table 2: List of the 34 CMIP6 GCMs used in this study together with the annual mean total GrIS precipitation for 1971–2000 and the change in total precipitation 2071–2100 relative to 1971–2000. Also given are the ensemble median values. The names in bold face are the GCMs downscaled by the RCMs. We have restricted the model selection and only using one ensemble member per GCM.

2.2 Observations and reanalysis

There are limited long-term observations of precipitation in Greenland and observed precipitation, particularly solid, is notoriously difficult to accurately measure (Allerup et al., 1997). Nevertheless, corrected datasets from automatic weather stations (AWS) operated by the Danish Meteorological Institute (DMI) have long time series that have been previously used to evaluate climate models (Huai et al., 2025; Boberg et al., 2018, Huai et al., 2021). On the GrIS, the PROMICE (Fausto et al., 2021) and GC-Net (Steffen and Box, 2001) networks of AWS assess surface height changes, using two or three different techniques, but these are hard to compare with precipitation in a climate model as they measure a different variable affected by for example, melt, firn densification and drifting snow processes. We have therefore chosen to concentrate on using the observed precipitation from the DMI AWS. The station data are undercatch corrected using the mean correction factors and mean rainfall fractions from Huai et al. (2021).

The Copernicus Arctic Regional Reanalysis (CARRA; Yang et al., 2020) is available from 1991 onward for two Arctic regions where one covers Greenland. CARRA data have a horizontal grid spacing of 2.5 km compared with the European Center for Medium-range Weather Forecasts fifth-generation reanalysis (ERA5) dataset at 31 km. Compared with ERA5, CARRA includes a number of improvements such as a larger set of local observations, a more realistic ice mask and coastline mask, a satellite derived glacier albedo dataset and high resolution sea surface temperatures and sea ice concentrations. The CARRA outperforms ERA5 when comparing the two datasets with in-situ observations of a range of variables including snowfall, snow depth, pressure, temperature and wind speeds across the Arctic (Køltzow al., 2022).

Eleven RCM simulations (historical 1991–2014 and SSP5-8.5 for 2015–2022) are validated against CARRA and observations for precipitation from seven stations with at least 10 000 daily measurements (out of a maximum of 11 688) for the 32-year period 1991–2022. The stations (see Figure 1) are located along the south-western and eastern coast of Greenland.





125 The six drainage basins (see Figure 1a) are taken from Rignot and Mouginot (2012), who used ice surface velocity maps from satellite radar interferometry data to divide the GrIS into six subregions of similar size.

2.2 Model evaluation

Figure 2a shows the mean annual precipitation for the CARRA dataset for 1991–2022, with values exceeding 2000 mm year⁻¹ in the southeast and southwest whereas the northern part of the GrIS is very dry with values below 200 mm year⁻¹ in large areas. Figure 2b to Figure 2l show the relative model difference for the eleven RCM simulations with respect to CARRA. We see similar patterns for all models with large areas with negative difference in the central parts of the GrIS and smaller areas with positive difference along the outer part of the GrIS. Four of the MAR models (Figure 2f to 2i) show a large positive difference in region NW and NO.

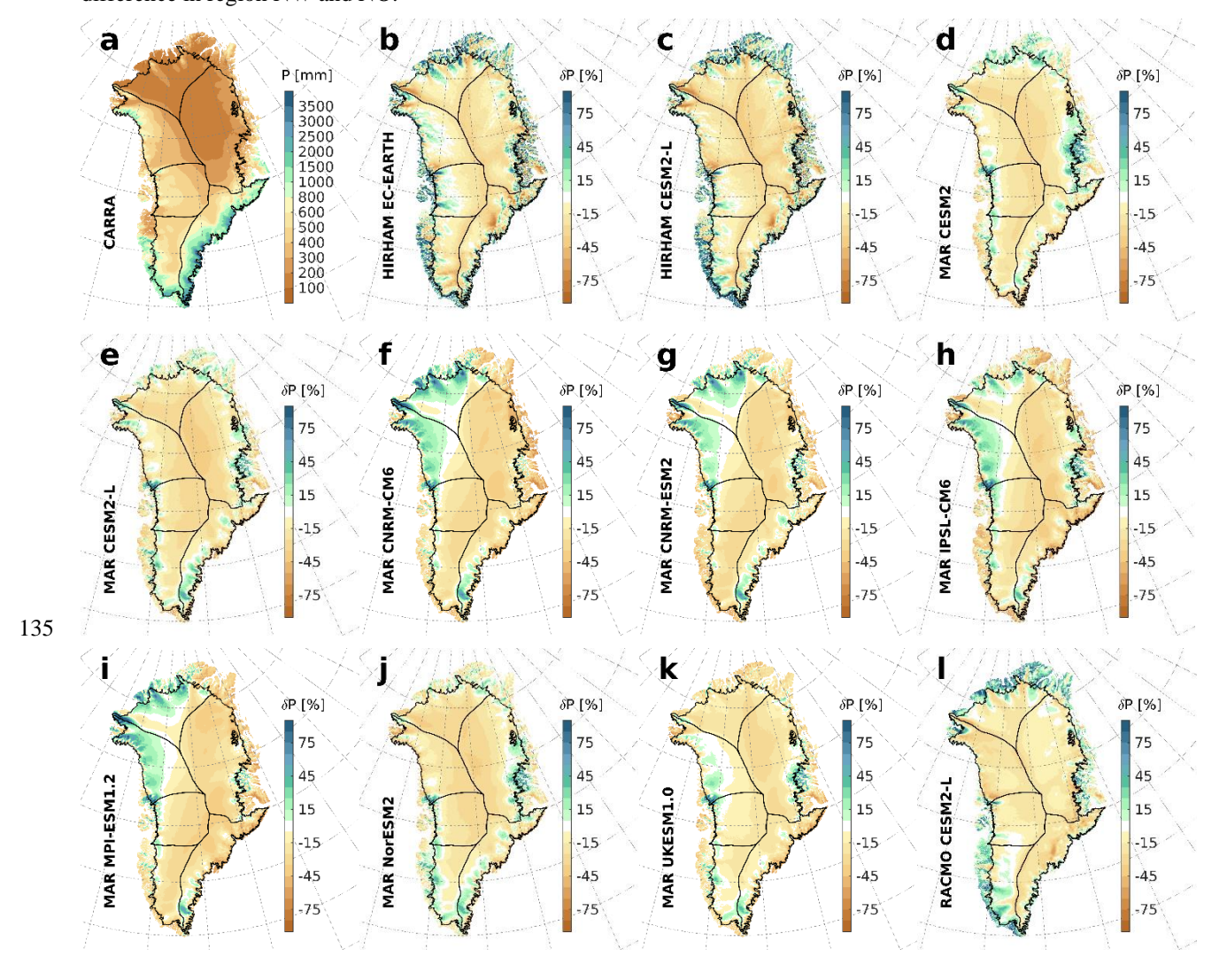






Figure 2: Mean annual precipitation for 1991–2022 by CARRA (a) and the model difference relative CARRA for HIRHAM/EC-EARTH (b), HIRHAM/CESM2-L (c), MAR/CESM2 (d), MAR/CESM2-L (e), MAR/CNRM-CM6 (f), MAR/CNRM-ESM2 (g), MAR/IPSL-CM6 (h), MAR/MPI-ESM1.2 (i), MAR/NorESM2 (j), MAR/UKESM1.0 (k) and RACMO/CESM2-L (l). For the RCM data, 1991–2014 is taken from the historical run and 2015–2022 is taken from the SSP5-8.5 scenario run. Black contour lines show the six drainage basins.

Figure 3 compares station observations of precipitation with CARRA and the eleven RCM models for the grid point closest to the weather stations (cf. Figure 1a). The HIRHAM and RACMO values are close to the observed mean annual precipitation for stations 2 and 4–7 while some of the MAR models are underestimating. For station 1, RACMO is overestimating the annual precipitation while HIRHAM and RACMO are overestimating for station 3. CARRA is performing well for all stations with somewhat lower values for stations 2 and 4. The two rightmost columns of Table 1 give the RMSE and mean bias for CARRA and the eleven RCM simulations, showing low RMSE values and low mean bias for the HIRHAM simulations and relatively high RMSE and negative bias for the MAR simulations.

CARRA models different climate variables well compared with ERA5 (Isaksen et al., 2022; Box et al., 2023; Køltzow et al., 2022). However, when comparing CARRA with station observations (see Figure 3 and Table 1) and RCM output, there are no clear evidence justifying a bias adjustment of the RCM data towards CARRA. Instead, we will use the raw model output in this study.

155

145





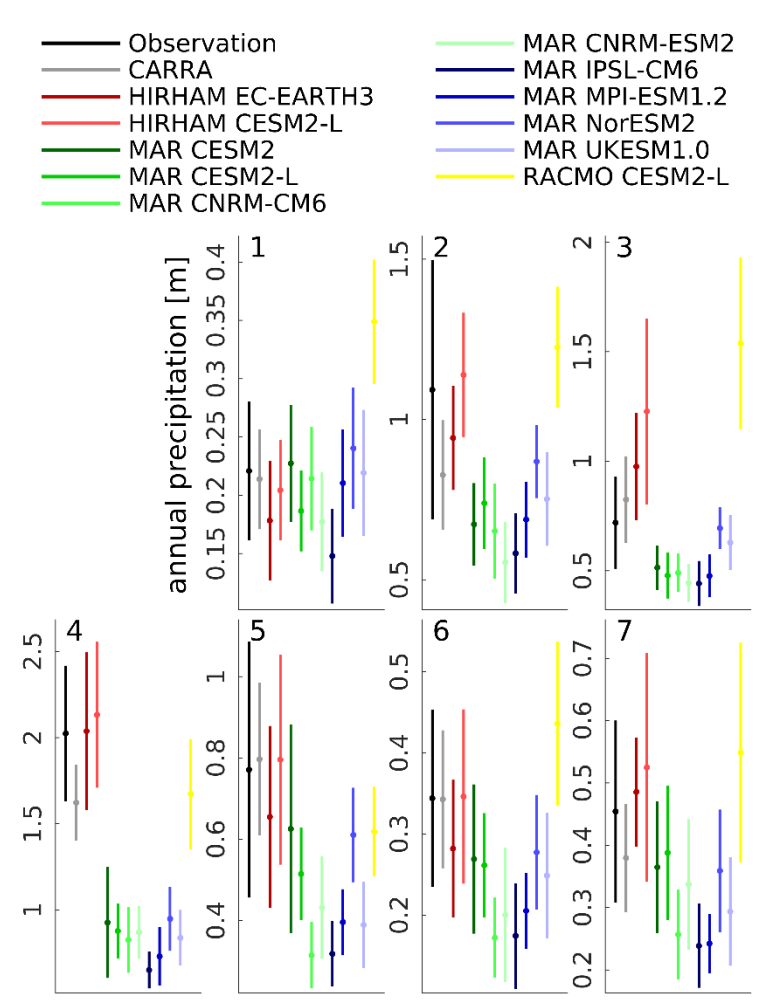


Figure 3: Mean annual precipitation for 1991–2022 (dots) for seven weather station locations (cf. Figure 1), showing observations, CARRA, two HIRHAM simulations, eight MAR simulations and one RACMO simulation. For the RCM data, 1991–2014 is taken from the historical run and 2015–2022 is taken from the SSP5-8.5 scenario run. The vertical lines show the standard deviation of the 32 yearly precipitation sums. The precipitation for CARRA and the HIRHAM, MAR and RACMO simulations are taken from the land grid point closest to the AWS locations.

3 Results

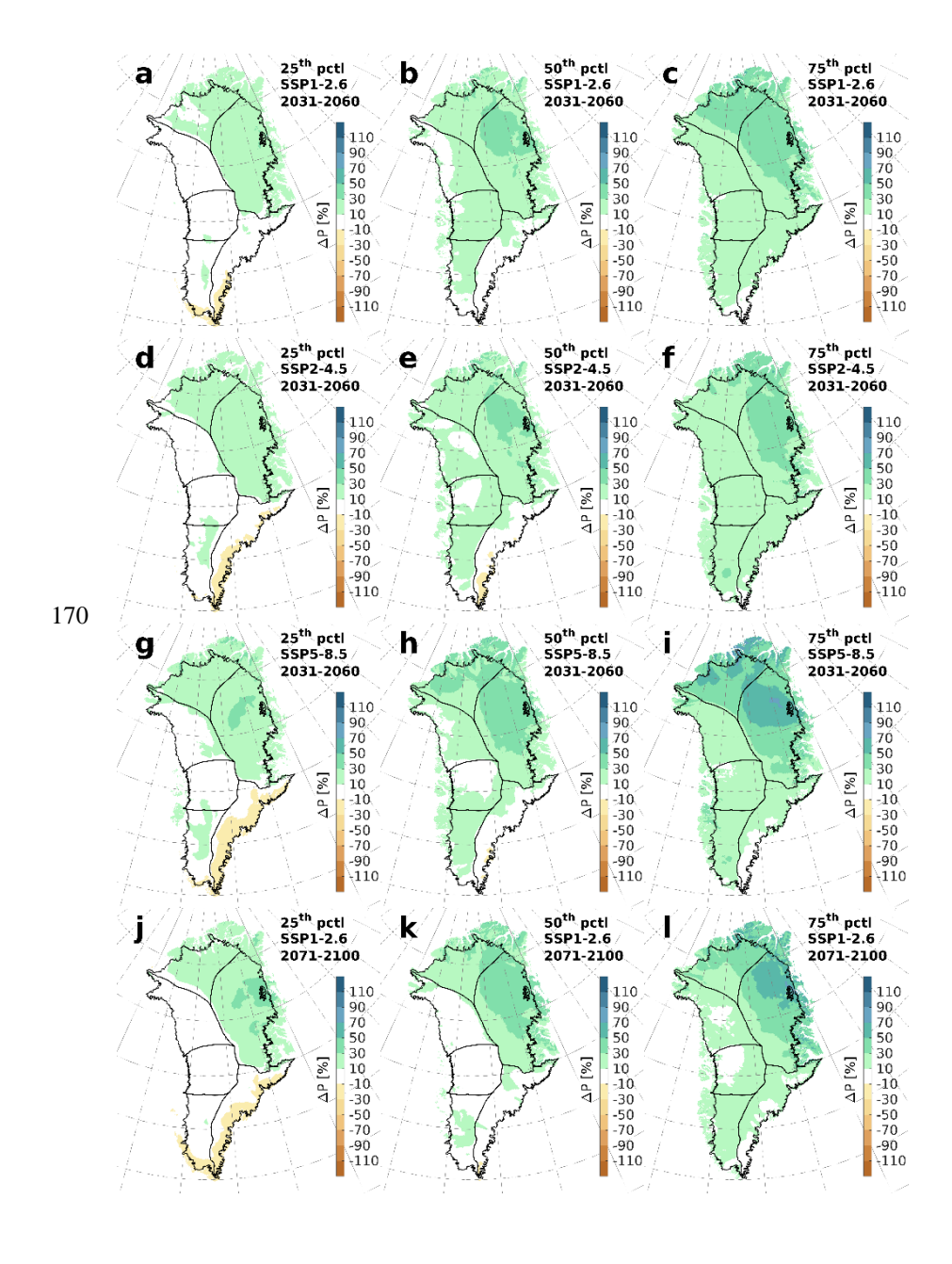
160

165

Figure 4 shows the model spread of the relative change in precipitation for a mid-century and an end of the century period relative to 1971–2000 using the RCM ensemble for all three SSP scenarios. In the middle of the century (Figure 4a to 4i) we see that the south-east shows smaller changes compared with the rest of the GrIS. Large parts of the interior are getting wetter, with the largest change in the north-east part of Greenland. Toward the end of the century (Figure 4j to 4r) we see an overall amplification of the mid-century signal with a high relative change in the northeast and a low relative change in the southeast.











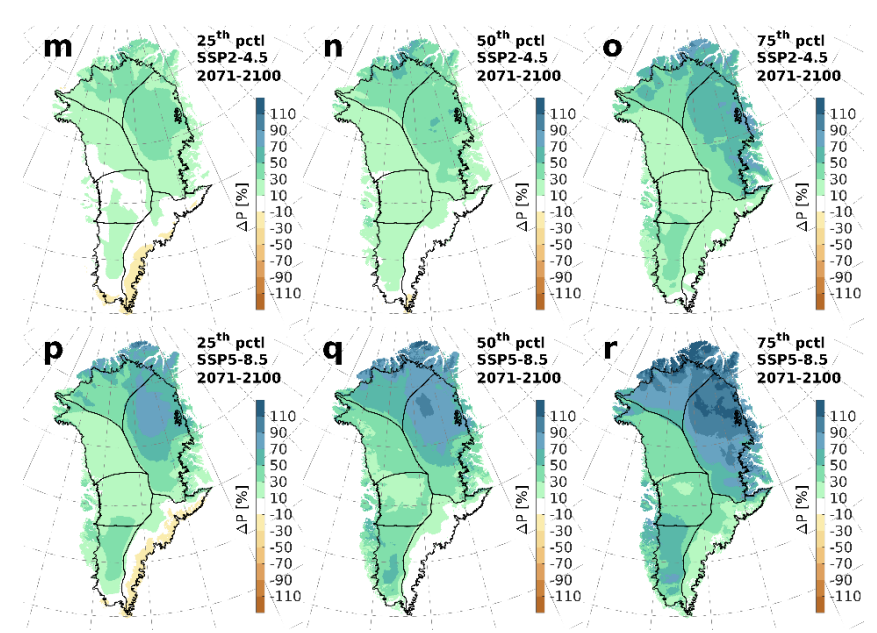
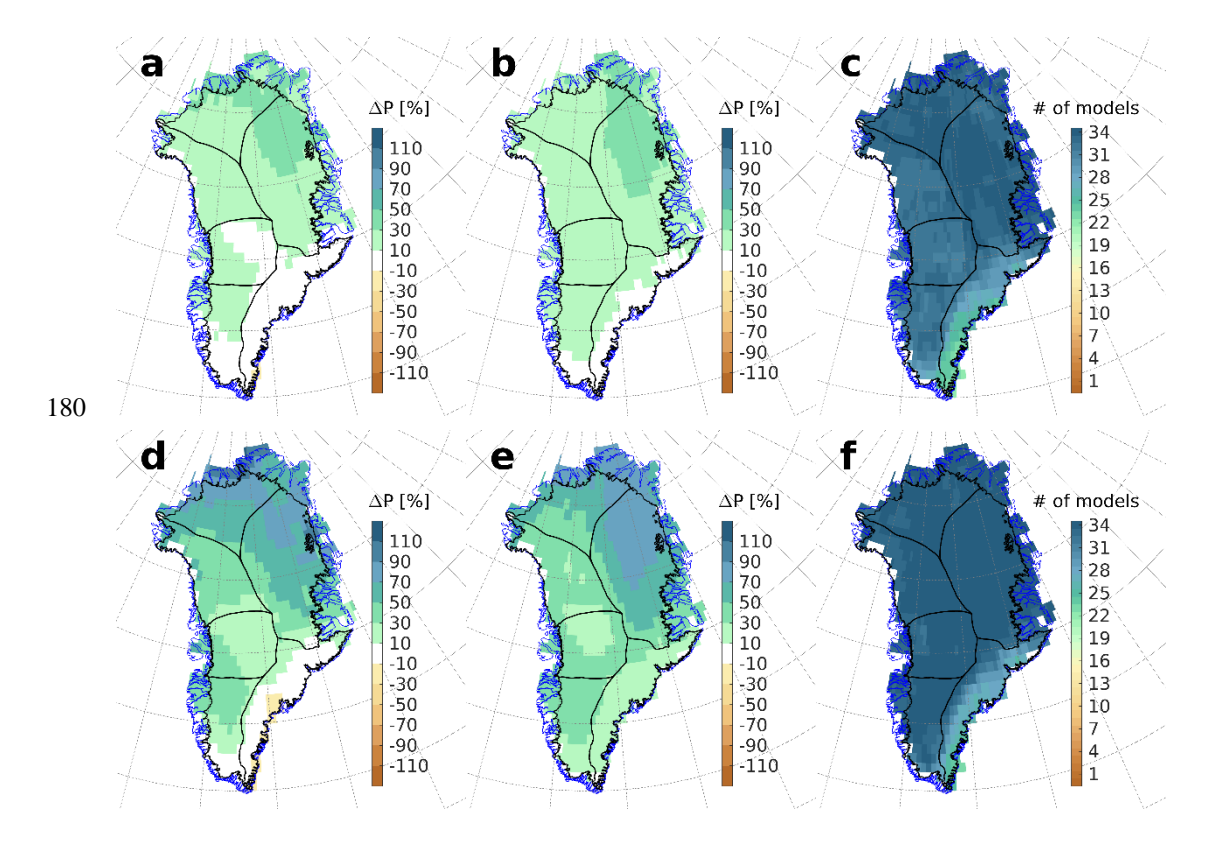


Figure 4: Relative change in Greenland precipitation using the RCM ensembles for SSP1-2.6 (panels a-c and j-l), SSP2-4.5 (panels d-f and m-o) and SSP5-8.5 (panels g-i and p-r). Panels a-i are for 2031-2060 relative 1971-2000 and panels j-r are for 2071-2100 relative 1971-2000. First column represents the 25th percentile, second column is the median and the third column represents the 75th percentile.





190

195

200

205



Figure 5: Ensemble median relative change in precipitation using the subset of CMIP6 models used when downscaling the RCMs for 2031–2060 (a) and 2071–2100 (d) relative to 1971–2000 for the SSP5-8.5 scenario. The corresponding ensemble median relative change using the full set of 34 CMIP6 GCMs are shown in panels b and e for 2031–2060 and 2071–2100, respectively. The two panels c and f in the right column show number of CMIP6 models, using the full 34 model set, with a positive relative change in precipitation for 2031–2060 (c) and 2071–2100 (f) relative to 1971–2000 for the SSP5-8.5 scenario, respectively.

Figure 5a and 5d shows the ensemble mean relative change, using the eight CMIP6 GCMs downscaled by the RCMs (cf. Table 2), for the SSP5-8.5 scenario for 2031–2060 and 2071–2100 relative 1971–2000, respectively. Figure 5b and 5e give the corresponding maps when using the full 34 CMIP6 GCMs for the SSP5-8.5 scenario. Compared with the full model ensemble, the eight model ensemble have smaller changes for all six subregions but most pronounced for region SE. Also shown in Figure 5c and 5f are the number of CMIP6 models that show positive changes in precipitation for the mid-century and end of century. The CMIP6 ensemble show agreement for all drainage basins except for basin SE where about 6 of the 34 members show a negative change, in line with Huai et al. (2025).

Figure 6 shows the change from solid to liquid precipitation for the SSP5-8.5 scenario. This indicates that not only will there be an increase in precipitation in the future, but an increasing fraction of that will be rainfall, especially around the ice sheet margins. At the end of the century for the SSP5-8.5 scenario, we see that a large fraction of the precipitation is rainfall, especially in the south (basin SW, SE, and parts of CW; cf. Fig. 1a). As shown in Table 1, the ensemble median values for the total precipitation for the historical period and the two scenario periods (using SSP5-8.5) are 700, 754 and 852 Gt over the GrIS. The corresponding values for snowfall are 663 (95% of the total precipitation), 683 (91%) and 687 Gt (81%). By the end of the 21st century, using the SSP5-8.5 scenario, we expect to have about 20% of the total precipitation in liquid form on the GrIS.

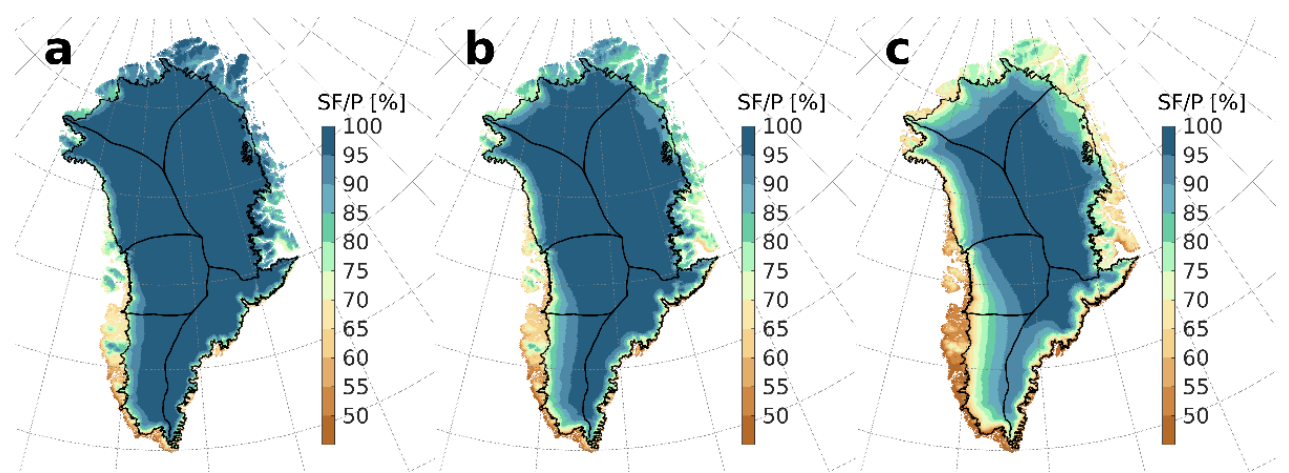


Figure 6: Ensemble median snowfall fraction of total precipitation in Greenland, using the eleven-model ensemble for the historical period 1971–2000 (a) and the two SSP5-8.5 scenario periods 2031–2060 (b) and 2071–2100 (c).



220

225



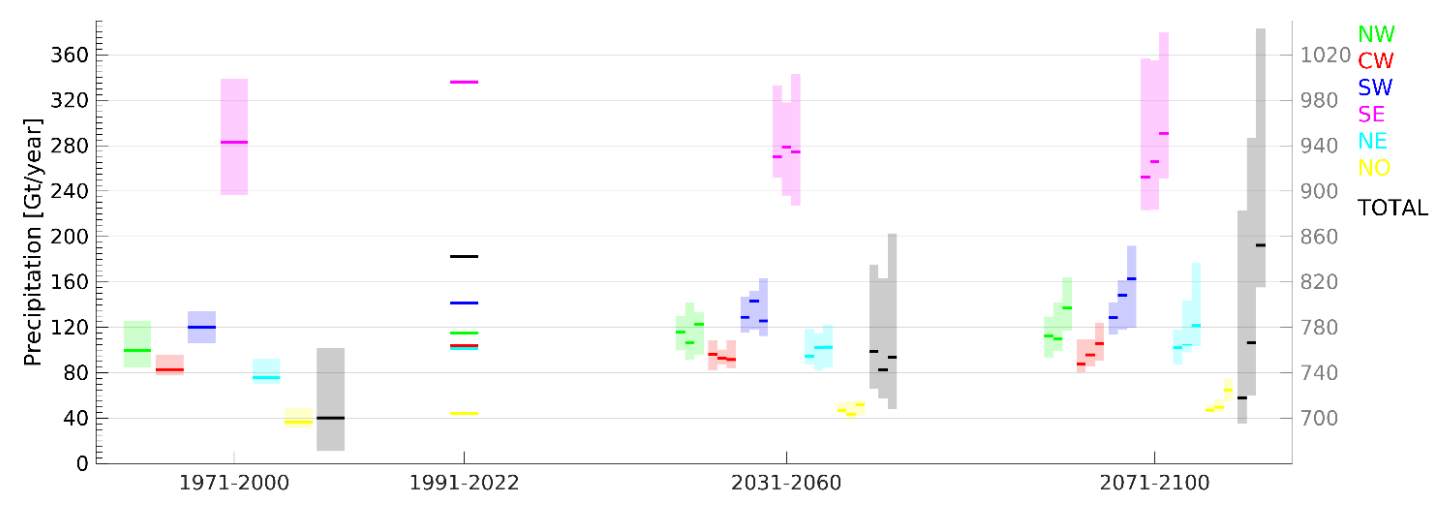


Figure 7: Mean precipitation (in Gt per year) for the RCM simulations over the six drainage basins and the full GrIS for the historical period 1971–2000, for CARRA (1991–2022) and the scenario periods 2031–2060 and 2071–2100. The horizontal lines denote the ensemble median while the vertical bars show the model spread. For the two scenario periods the bars are split into three segments: the left for SSP1-2.6, the middle for SSP2-4.5 and the right for SSP5-8.5. The y axis to the right is used for the full GrIS (black) while the values for the six individual drainage basins are given by the y axis to the left.

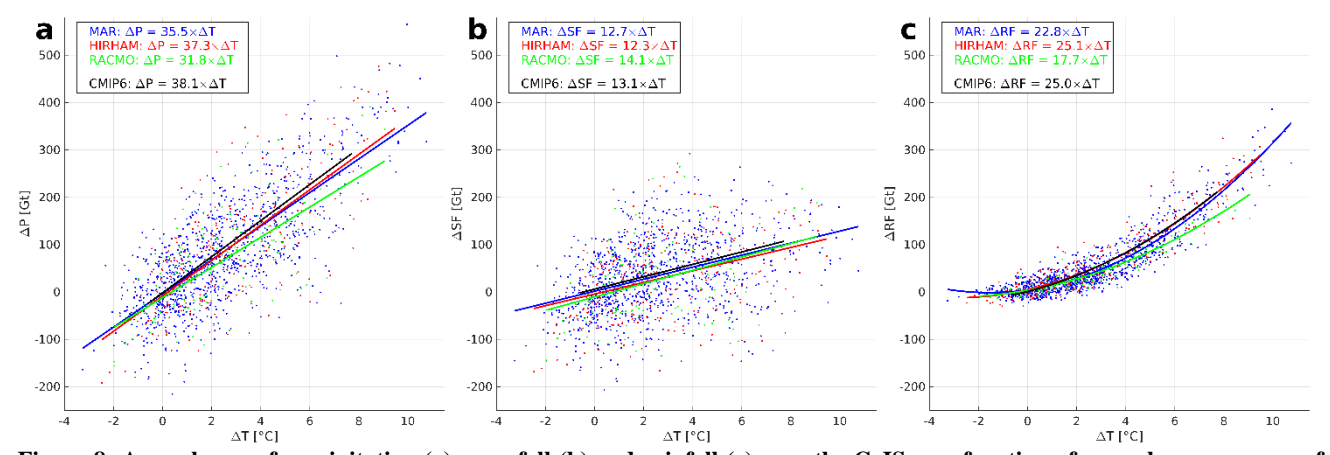


Figure 8: Annual sum of precipitation (a), snowfall (b) and rainfall (c) over the GrIS as a function of annual mean near-surface temperature for the period 1971–2100, using the SSP5-8.5 scenario, with respect to the 1971–2000 mean. The data are separated for each RCM (MAR: blue, HIRHAM: red and RACMO: green), including a least square fit (linear for a and b, second degree polynomial for c). Also shown is the linear fit to the 34 model CMIP6 ensemble mean values (black).

Figure 7 shows the annual total precipitation for the six drainage basins as well as for the total GrIS for CARRA and the RCM simulations. The vertical extent of each bar represents the model spread for each basin and for the two scenario periods the bar is split into three segments to show the difference between the three SSPs. The largest uncertainties are, as expected, found in region SE. There is no clear difference between the SSPs for the 2031–2060 period while the 2071–2100 period has a clear difference in the ensemble median. The CARRA values match the higher end of the model spread for each basin, giving a total annual amount that is significantly higher than any of the other models.



235

240

245

250



A warmer atmosphere has an exponentially higher saturation specific humidity (can hold more water vapour), termed the Clausius-Clapeyron relationship with about a 7% increase per degree warming (Trenberth et al. 2003). Figure 8a shows the relationship between annual temperature and annual precipitation over the GrIS for the three RCMs using data for the historical period and the SSP5-8.5 scenario only to have a more uniform distribution of the data points. Here we see that the integrated precipitation over the GrIS increases with 31.8, 35.5, and 37.3 Gt per degree change in temperature for RACMO, MAR and HIRHAM respectively. Figure 8b and 8c shows that the increase in rainfall per degree of warming is larger than the increase in snowfall per degree warming. Snowfall is expected to increase by about 13 Gt per degree of warming while rainfall is expected to increase with above 20 Gt per degree of warming during the 21st century but with a non-linear trend indicating a much higher value at the end of the century.

4 Discussion

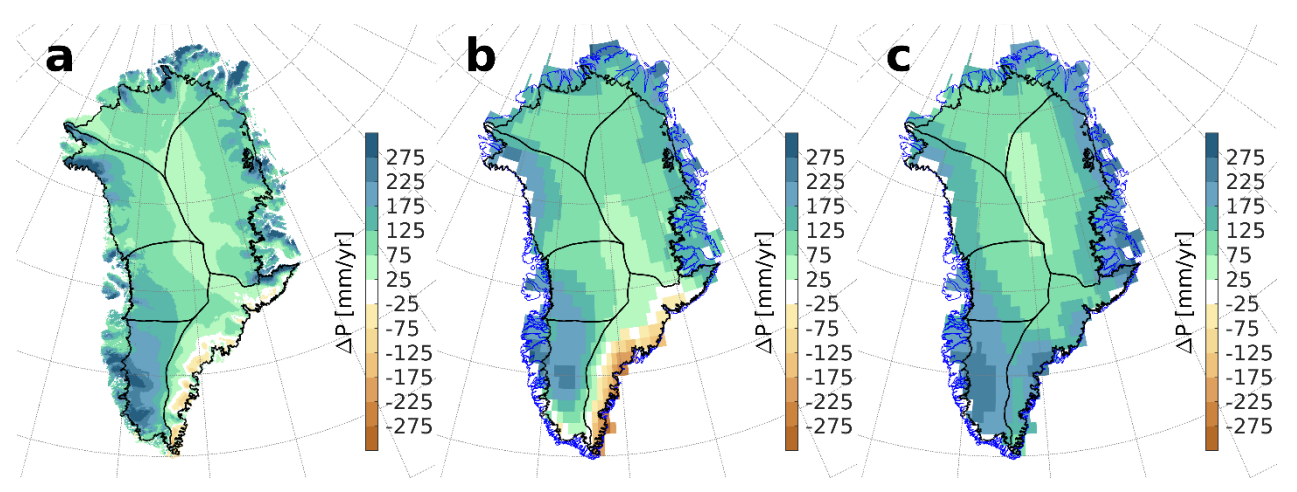


Figure 9: Ensemble median absolute change in precipitation for SSP5-8.5 for 2071–2100 relative 1971–2000 using the RCM ensemble (a), the subset of downscaled GCMs (b) and the full set of GCMs (c).

4.1 Implications for mass budget

Using an ensemble of high resolution RCM simulations for the SSP1-2.6/SSP2-4.5/SSP5-8.5 scenarios, we predict an increase of precipitation on the GrIS during the 21st century, though with a change in the relative distribution of precipitation as well as a change in the phase. The largest relative differences are predicted in the north east of Greenland, where all models see a marked increase. In the southeast by contrast, the RCM ensemble median give relative changes close to zero (cf. Figure 4 and Figure 7). Results from the GCM ensemble from CMIP6 (cf. Figure 5) show that both the north east and south east signals are robust across most models. The RCMs follow the forcing GCM climate in this respect but their higher resolution shows more detail on the local scale. In absolute terms (cf. Figure 9a), for the end of century SSP5-8.5 scenario the largest changes are

© Author(s) 2025. CC BY 4.0 License.





expected, using the RCM ensemble, in the south west of Greenland with values exceeding 200 mm yr⁻¹ and along the outer edge of the GrIS with values between 100 and 200 mm yr⁻¹ (except for the south east with values close to 0). A similar pattern is seen using the subset of GCMs (cf. Figure 9b) but with even lower (and negative) values in the south east. For the full set of GCMs (cf. Figure 9c) we see positive changes for all of the GrIS with the highest values in the south west and south east.

255

260

265

The phase distinction of precipitation is important because rainfall serves as a crucial climate indicator in polar regions and plays a multifaceted role in cryospheric processes. When rain falls on snow or ice surfaces, its infiltration not only contributes directly to surface melt, but also initiates a sequence of physical changes in the snowpack. The freezing of rainwater within the firn releases latent heat, which further accelerates melting by warming the surrounding ice and snow. In addition, rainfall events lower the surface albedo making the surface more susceptible to future melting due to increased absorption of solar radiation (Noël et al., 2022; Firn Symposium team, 2024; Gilbert et al., 2025).

By the end of the century, the GrIS is expected to receive between 40 and 170 Gt more precipitation annually, depending on the climate scenario (cf. Table 1), an increase between 6 and 24% compared to the present day. Glaude et al. (2024) however, show from some of the same simulations as we analyse here, that the melt and runoff is projected to increase by a much larger amount (around 2,000 Gt per year in runoff). The increase in precipitation will therefore unlikely to be enough to offset ablation losses.

4.2 Sources of spread in precipitation projections

Huai et al. (2025) used CMIP6 GCM outputs for the SSP5-8.5 scenario and found a northeastward shift of the Icelandic low leading to lower precipitation amounts in southeast Greenland. The future location of the Icelandic low has therefore an important influence on precipitation changes over southeast Greenland, as CMIP6 models have some important biases in the Iceland Low and representation of the North Atlantic Oscillation.

CARRA has shown clear advantages to other reanalysis products (Køltzow et al., 2022) but it appears to overestimate precipitation in the southeast of Greenland (cf. Figure 3 and Figure 7), though performs better in other regions. This may simply reflect the local conditions around the observation sites, which are typically located in topographically complex terrain, difficult to capture even at 2.5 km resolution. To accurately capture extreme weather events in Greenland, DMI use a sub-km resolution model for numerical weather prediction purposes (Yang, 2018; Yang, 2019).

280 U

Using the mean values of total precipitation, separated by RCM, in Table 1 for the period 1971–2000 together with the relationship between precipitation and temperature in Figure 8, we get 4.9%, 5.1% and 4.5% increase in precipitation per Kelvin for HIRHAM, MAR and RACMO, respectively. These values are lower than the app. 7% K⁻¹ predicted by the Clausius-Clapeyron relationship (Trenberth et al., 2003). However, the near-surface temperature is not an accurate measure of the

© Author(s) 2025. CC BY 4.0 License.





vertically weighted atmospheric temperature where the moisture resides. Moreover, the total GrIS precipitation is for an important part topographically forced, i.e. very sensitive to changes in the large-scale circulation. Bochow et al. (2024) used 32 GCMs within the CMIP6 project and found a mean value of 6% K⁻¹ for the GrIS but with a strong spatial dependence. A 5% increase in precipitation per degree warming over the GrIS were found by Gregory and Huybrechts (2006) and by Fettweis et al. (2013).

Figure 6 shows that a significant fraction of future precipitation, particularly over the southern GrIS, will fall as rain. On the broad scale, rain replacing snow implies enhanced ablation over the GrIS due to surface energy budget and firn processes (Box et al., 2023). On a local to regional scale, increased rainfall, particularly close to the end of the melt season, has also been shown to affect outlet glacier dynamics (Doyle et al., 2014) with local short-lived increases in ice velocity. The CMIP6 GCMs are unlikely to capture this transition from snow to rain, and along with the higher resolution show how RCMs add value to the GCMs when considering future climate change. Zhang et al. (2024) used 21 CMIP6 models for the SSP5-8.5 scenario giving a projected annual increase in precipitation over the GrIS of 280 Gt for 2071–2100 relative 1986–2005. The RCM ensemble median gives 170 Gt with individual model values ranging from 120 to 360 Gt.

5 Conclusions

300

305

The GrIS faces a wetter future in all regions, with as a possible exception the southeast. The fraction of rain relative to the total precipitation increases with time during the 21st century. Our analysis clearly shows a linear relationship between annual precipitation amounts and annual mean temperature as well as a dependency on SSP. We also see a dependency on driving model; when all three RCMs downscale the same GCM (CESM2-L) we obtain similar results on change in precipitation for both scenario periods (cf. Table 1). For the historical period, the different MAR simulations show similar results while HIRHAM, and to some extent RACMO, present different characteristics (cf. Figure 3). At the end of the century, HIRHAM, driven by EC-Earth3, and MAR, driven by IPSL-CM6 and UKESM1.0, give much higher changes in precipitation over the GrIS than the other RCM simulations, indicating a dependency on the choice of GCM. The more detailed topography from the higher resolution RCMs shows a complexity in the distribution of precipitation suggesting that using emulation techniques on RCM output to expand future ensembles of climate simulations is feasible.

Acknowledgments

Fredrik Boberg, Nicolaj Hansen and Ruth Mottram are supported by the Danish State through the National Centre for Climate Research (NCKF) and also supported by the European Union's Horizon 2020 project PROTECT (grant no. 869304); furthermore, Nicolaj Hansen has been supported by the Novo Nordisk Foundation project PRECISE (grant no. NNF23OC0081251).

© Author(s) 2025. CC BY 4.0 License.



EGUsphere Preprint repository

Author contributions

RM, FB and NH designed the study. FB performed the HIRHAM simulations, the data collection and the analysis. XF and MvdB provided the MAR and RACMO data, respectively. FB wrote the paper with contributions from all co-authors.

Data availability

All GCM, RCM, CARRA and station observation data used in this study will be made available upon request. CARRA data can be downloaded from the Copernicus Arctic Regional Reanalysis webpage at https://climate.copernicus.eu/copernicus-arctic-regional-reanalysis-service. The drainage basin information can be downloaded from http://imbie.org/imbie-2016/drainage-basins/.

References

335

Allerup, P., Madsen, H., and Vejen, F.: A comprehensive model for correcting point precipitation, Nordic Hydrology, 28, 1–20, 1997.

Boberg, F., Langen, P. L., Mottram, R. H., Christensen, J. H., and Olesen, M.: 21st-century climate change around Kangerlussuaq, west Greenland: From the ice sheet to the shores of Davis Strait, Arctic, Antarctic, and Alpine Research, 50(1), https://doi.org/10.1080/15230430.2017.1420862, 2018.

Boberg, F., Mottram, R., Hansen, N., Yang, S., and Langen, P. L.: Uncertainties in projected surface mass balance over the polar ice sheets from dynamically downscaled EC-Earth models, The Cryosphere, 16, 17–33, https://doi.org/10.5194/tc-16-17-2022, 2022.

Bochow, N., Poltronieri, A., and Boers, N.: Projections of precipitation and temperatures in Greenland and the impact of spatially uniform anomalies on the evolution of the ice sheet, The Cryosphere, 18, 5825–5863, https://doi.org/10.5194/tc-18-5825-2024, 2024.

Box, J. E., Hubbard, A., Bahr, D.B. et al.: Greenland ice sheet climate disequilibrium and committed sea-level rise. Nat. Clim. Chang., 12, 808–813, https://doi.org/10.1038/s41558-022-01441-2, 2022.



345

355



- Box, J. E., Nielsen, K. P., Yang, X., Niwano, M., Wehrlé, A., van As, D., et al.: Greenland ice sheet rain climatology, extremes and atmospheric river rapids, Meteorological Applications, 30(4), e2134, https://doi.org/10.1002/met.2134, 2023.
 - Doyle, S. H., Hubbard, A., Fitzpatrick, A. A. W., van As, D., Mikkelsen, A. B., Pettersson, R., and Hubbard, B.: Persistent flow acceleration within the interior of the Greenland ice sheet, Geophysical Research Letters, 41(3), 899–905. https://doi.org/10.1002/2013GL058933, 2014.
 - Döscher, R., Acosta, M., Alessandri, A., Anthoni, P., Arsouze, T., Bergman, T., Bernardello, R., Boussetta, S., Caron, L.-P., Carver, G., Castrillo, M., Catalano, F., Cvijanovic, I., Davini, P., Dekker, E., Doblas-Reyes, F. J., Docquier, D., Echevarria, P., Fladrich, U., Fuentes-Franco, R., Gröger, M., v. Hardenberg, J., Hieronymus, J., Karami, M. P., Keskinen, J.-P., Koenigk, T., Makkonen, R., Massonnet, F., Ménégoz, M., Miller, P. A., Moreno-Chamarro, E., Nieradzik, L., van Noije, T., Nolan, P.,
- O'Donnell, D., Ollinaho, P., van den Oord, G., Ortega, P., Prims, O. T., Ramos, A., Reerink, T., Rousset, C., Ruprich-Robert, Y., Le Sager, P., Schmith, T., Schrödner, R., Serva, F., Sicardi, V., Sloth Madsen, M., Smith, B., Tian, T., Tourigny, E., Uotila, P., Vancoppenolle, M., Wang, S., Wårlind, D., Willén, U., Wyser, K., Yang, S., Yepes-Arbós, X., and Zhang, Q.: The EC-Earth3 Earth system model for the Coupled Model Intercomparison Project 6, Geosci. Model Dev., 15, 2973–3020, https://doi.org/10.5194/gmd-15-2973-2022, 2022.
 - Fausto, R. S., van As, D., Mankoff, K. D., Vandecrux, B., Citterio, M., Ahlstrøm, A. P., Andersen, S. B., Colgan, W., Karlsson, N. B., Kjeldsen, K. K., Korsgaard, N. J., Larsen, S. H., Nielsen, S., Pedersen, A. Ø., Shields, C. L., Solgaard, A. M., and Box, J. E.: Programme for Monitoring of the Greenland Ice Sheet (PROMICE) automatic weather station data, Earth Syst. Sci. Data, 13, 3819–3845, https://doi.org/10.5194/essd-13-3819-2021, 2021.
 - Fettweis, X., Franco, B., Tedesco, M., van Angelen, J. H., Lenaerts, J. T. M., van den Broeke, M. R., and Gallée, H.: Estimating the Greenland ice sheet surface mass balance contribution to future sea level rise using the regional atmospheric climate model MAR, The Cryosphere, 7, 469–489, https://doi.org/10.5194/tc-7-469-2013, 2013.
- 365 Firn Symposium team, The, Firn on ice sheets, Nat. Rev. Earth Environ., 5, 79–99, https://doi.org/10.1038/s43017-023-00507-9, 2024.
- Gilbert, E., Pishniak, D., Torres, J. A., Orr, A., Maclennan, M., Wever, N., and Verro, K.: Extreme precipitation associated with atmospheric rivers over West Antarctic ice shelves: insights from kilometre-scale regional climate modelling. The Cryosphere, 19(2), 597-618, 2025.
 - Glaude, Q., Noel, B., Olesen, M., Van den Broeke, M., van de Berg, W. J., Mottram, R., et al.: A factor two difference in 21st-century Greenland ice sheet surface mass balance projections from three regional climate models under a strong warming



385



scenario (SSP5-8.5),

375 Geophysical Research Letters, 51, e2024GL111902, https://doi.org/10.1029/2024GL111902, 2024.

Gregory J. M. and Huybrechts P.: Ice-sheet contributions to future sea-level change, Phil. Trans. R. Soc. A., 364, 1709–1732, http://doi.org/10.1098/rsta.2006.1796, 2006.

Hofer, S., Lang, C., Amory, C. et al.: Greater Greenland Ice Sheet contribution to global sea level rise in CMIP6. Nat. Commun., 11, 6289, https://doi.org/10.1038/s41467-020-20011-8, 2020.

Huai, B., Van Den Broeke, M. R., Reijmer, C. H., and Cappellen, J.: Quantifying Rainfall in Greenland: A Combined Observational and Modeling Approach, Journal of Applied Meteorology and Climatology, 60(8), 1171–1188. https://doi.org/10.1175/JAMC-D-20-0284.1, 2021.

Huai, B., Ding, M., van den Broeke, M.R. et al.: Future large-scale atmospheric circulation changes and Greenland precipitation, npj Clim. Atmos. Sci., 8, 10, https://doi.org/10.1038/s41612-025-00899-z, 2025.

Huybrechts, P., Letreguilly, A., Reeh, N.: The Greenland ice sheet and greenhouse warming, Paleogeogr. Paleoclim. 390 Paleoecol., 89, 399–412, 1991.

Isaksen, K., Nordli, Ø., Ivanov, B. et al.: Exceptional warming over the Barents area, Sci. Rep. 12, 9371, https://doi.org/10.1038/s41598-022-13568-5, 2022.

395 Køltzow, M., Schyberg, H., Støylen, E., and Yang, X.: Value of the Copernicus Arctic Regional Reanalysis (CARRA) in representing near-surface temperature and wind speed in the north-east European Arctic, Polar Research, 41, https://doi.org/10.33265/polar.v41.8002, 2022.

Noël, B., van de Berg, W. J., van Wessem, J. M., van Meijgaard, E., van As, D., Lenaerts, J. T. M., Lhermitte, S., Kuipers Munneke, P., Smeets, C. J. P. P., van Ulft, L. H., van de Wal, R. S. W., and van den Broeke, M. R.: Modelling the climate and surface mass balance of polar ice sheets using RACMO2 Part 1: Greenland (1958–2016), The Cryosphere, 12, 811–831, https://doi.org/10.5194/tc-12-811-2018, 2018.



410

420



Noël, B., van Kampenhout, L., van de Berg, W. J., Lenaerts, J. T. M., Wouters, B., and van den Broeke, M. R.: Brief communication: CESM2 climate forcing (1950–2014) yields realistic Greenland ice sheet surface mass balance, The Cryosphere, 14, 1425–1435, https://doi.org/10.5194/tc-14-1425-2020, 2020.

Noël, B., Lenaerts, J. T., Lipscomb, W. H., Thayer-Calder, K., and van den Broeke, M. R.: Peak refreezing in the Greenland firn layer under future warming scenarios, Nat. Commun., 13, 6870, https://doi.org/10.1038/s41467-022-34524-x, 2022.

Rignot, E. and Mouginot, J.: Ice flow in Greenland for the International Polar Year 2008-2009: ICE FLOW GREENLAND 2009, Geophysical Research Letters, 39, https://doi.org/10.1029/2012GL051634, 2012.

Roeckner, E., Bäuml, G., Bonaventura, L., Brokopf, R., Esch, M., Giorgetta, M., Hagemann, S., Kirchner, I., Kornblueh, L.,
415 Manzini, E., Rhodin, A., Schlese, U., Schulzweida, U. and Tompkins, A.: The atmospheric general circulation model
ECHAM5. Part 1. Model description, Report no. 349, Max-Planck-Institut für Meteorologie (MPI-M), 2003.

Steffen, K. and Box, J.: Surface climatology of the Greenland Ice Sheet: Greenland Climate Network 1995–1999, J. Geophys. Res.-Atmos., 106, 33951–33964, https://doi.org/10.1029/2001jd900161, 2001.

Trenberth, K. E., Dai, A., Rasmussen, R. M., and Parsons, D. B.: The changing character of precipitation, Bull. Am. Meteorol. Soc., 84, 1205–1217, 2003.

Undén, P., Rontu, L., Järvinen, H., Lynch, P., Calvo, J., Cats, G., Cuxart, J., Eerola, K, Fortelius, C., Garcia-Moya, J. A., Jones,
C., Lenderlink, G., McDonald, A., McGrath, R., Navascues, B., Woetman Nielsen, N., Ødegaard, V., Rodrigues, E.,
Rummukainen, M., Room, R., Sattler, K., Hansen Sass, B., Savijärvi, H., Wichers Schreur, B., Sigg, R. The, H. and Tijm, A.:
HIRLAM-5 Scientific Documentation. Scientific Report, 2002.

Yang, X.: Sub-km HARMONIE and on-demand setup for storm forecast, Joint ALADIN-HIRLAM Newsletter 10, pp 35–430 39, Jan 2018, 2018.

Yang, X.: TAS, an operational forecast model at hectometric scale. Joint ALADIN-HIRLAM Newsletter 12, pp 40–49, Jan 2019, 2019.

435 Yang X., Schyberg H., Palmason B., Bojarova J., Box J., Pagh Nielsen K., Amstrup B., Peralta C., Høyer J., Nielsen Englyst P., Homleid M. Køltzow M.A.Ø., Randriamampianina R., Dahlgren P., Støylen E., Valkonen T., Thorsteinsson S., Kornich





H., Lindskog M. and Mankoff K.: C3S Arctic regional reanalysis—full system documentation. Accessed on the internet at https://cds.climate.copernicus.eu/cdsapp#!/dataset/reanalysis-carra-single-levels?tab=doc on 1 November 2021, 2020.

Zhang, Q., Huai, B., Ding, M., Sun, W., Liu, W., Yan, J., Zhao, S., Wang, Y., Wang, Y., Wang, L., Che, J., Dou, J., Kang., L.: Projections of Greenland climate change from CMIP5 and CMIP6 Global Planet. Change, 232, Article 104340, 10.1016/j.gloplacha.2023.104340, 2024.